G-CSF partially mediates effects of sleeve gastrectomy on the bone marrow niche

Ziru Li, … , Clifford J. Rosen, Ormond A. MacDougald

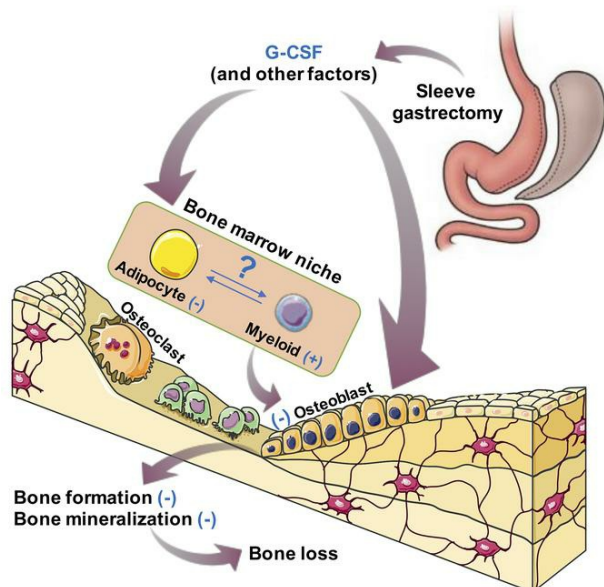Research Article   Bone biology   Endocrinology

Graphical abstract

G-CSF partially mediates effects of sleeve gastrectomy on the bone marrow niche

Ziru Li,[1] Julie Hardij,[1] Simon S. Evers,[2] Chelsea R. Hutch,[2] Sarah M. Choi,[3] Yikai Shao,[2] Brian S. Learman,[1] Kenneth T. Lewis,[1] Rebecca L. Schill,[1] Hiroyuki Mori,[1] Devika P. Bagchi,[1] Steven M. Romanelli,[1] Ki-Suk Kim,[2] Emily Bowers,[4] Cameron Griffin,[4] Randy J. Seeley,[2] Kanakadurga Singer,[4] Darleen A. Sandoval,[2] Clifford J. Rosen,[5] and Ormond A. MacDougald[1]

[1]Department of Molecular & Integrative Physiology, [2]Department of Surgery, [3]Department of Pathology, and [4]Department of Pediatrics and Communicable Diseases, University of Michigan Medical School, Ann Arbor, Michigan, USA. [5]Maine Medical Center Research Institute, Scarborough, Maine, USA.

Bariatric surgeries are integral to the management of obesity and its metabolic complications. However, these surgeries cause bone loss and increase fracture risk through poorly understood mechanisms. In a mouse model, vertical sleeve gastrectomy (VSG) caused trabecular and cortical bone loss that was independent of sex, body weight, and diet, and this loss was characterized by impaired osteoid mineralization and bone formation. VSG had a profound effect on the bone marrow niche, with rapid loss of marrow adipose tissue, and expansion of myeloid cellularity, leading to increased circulating neutrophils. Following VSG, circulating granulocyte–colony stimulating factor (G-CSF) was increased in mice, and was transiently elevated in a longitudinal study of humans. Elevation of G-CSF was found to recapitulate many effects of VSG on bone and the marrow niche. In addition to stimulatory effects of G-CSF on myelopoiesis, endogenous G-CSF suppressed development of marrow adipocytes and hindered accrual of peak cortical and trabecular bone. Effects of VSG on induction of neutrophils and depletion of marrow adiposity were reduced in mice deficient for G-CSF; however, bone mass was not influenced. Although not a primary mechanism for bone loss with VSG, G-CSF plays an intermediary role for effects of VSG on the bone marrow niche.

Introduction

The high incidence of obesity and type 2 diabetes mellitus represent important public health problems worldwide (1). According to the Centers for Disease Control, the incidence of obesity has increased to more than a third of the U.S. population, whereas severe obesity (BMI > 35 kg/m²) now affects more than 10% of individuals. Although the first line of treatment for obesity involves a multidisciplinary approach with behavioral and lifestyle modifications, long-term effects on weight loss and reduction of associated metabolic diseases are generally modest. Thus, weight loss surgery is now an integral component of clinical management of obese patients; in the U.S. alone, there were more than 200,000 bariatric surgeries performed in 2016 (2).

Although a variety of bariatric surgeries have been developed, vertical sleeve gastrectomy (VSG) currently accounts for more than half of the procedures performed, and is gaining in popularity (2). These procedures cause an impressive 15% to 30% reduction in body mass (3). Importantly, bariatric surgery improves glucose

tolerance and cardiovascular disease risk, effects that are largely independent of weight loss (4, 5). The mechanisms by which bariatric surgery improve glucose homeostasis, independent of weight loss, appear to be complex and involve energy expenditure, macronutrient preference, luminal composition of the gut (i.e., microbiota and bile acids), adaptation of the gastrointestinal lining, altered postprandial gut hormone secretions, increases in insulin-dependent and -independent glucose disposal, pancreas morphology, and absorption of micronutrient and minerals (6). Bariatric surgeries are associated with other on- and off-target side effects, including macro- and micronutrient malabsorption, hypoglycemia, anemia, rapid bone loss, and a higher fracture risk (7–10). Potential causes of bone loss independent of weight loss with VSG in humans and animal models have been explored, and include adaptation to unloading, abnormalities in calciotropic hormones, and altered gut and adipokine hormones (8, 11–15). However, definitive mechanisms for bone loss have not been determined.

There is increasing appreciation of important functional interactions between bone cells and other cell types within the marrow niche such as bone marrow adipocytes and hematopoietic cells (16, 17). Bone marrow is an enclosed system, and thus expansion of one cell type is often at the expense of others (16). Thus, mechanistic insights into how VSG causes bone loss may require a broader evaluation of the interactions among marrow components, particularly as exemplified by anemia caused by VSG (18).

Herein we report that cortical and trabecular bone loss following VSG is due to impaired osteoid mineralization and bone formation. Within the niche, VSG rapidly depletes bone marrow adipose tissue (BMAT) and expands myeloid cellularity and circulating neutrophils. One potential intermediary mechanism is gran-
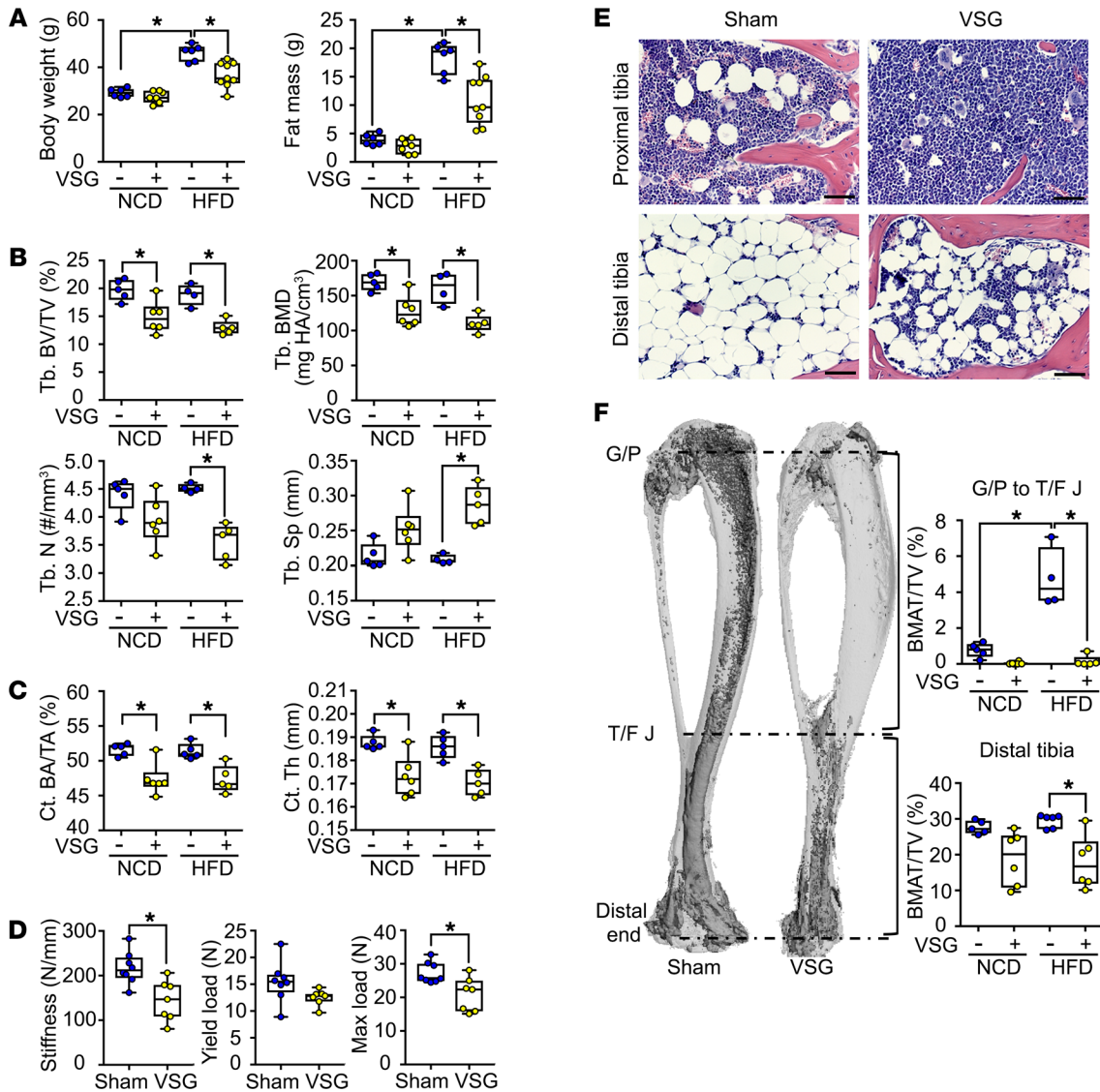
Figure 1. Loss of bone and BMAT after VSG is independent of mechanical unloading and diet. After consumption of HFD for 8 weeks, male C57BL/6J mice at 12 weeks of age received sham or VSG surgery. Each group was then fed NCD or HFD for a further 8 weeks. (**A**) Body weight and fat mass were measured before euthanasia ($n = 6$ for NCD+Sham; $n = 7$ for NCD+VSG; $n = 6$ for HFD+Sham, and $n = 9$ for HFD+VSG). (**B**) Tibial Tb. BV/TV, Tb. BMD, Tb. N, and Tb. Sp were measured with μCT. (**C**) Mid-tibial Ct. BA/TA and Ct. Th ($n = 5$ for NCD+Sham; $n = 6$ for NCD+VSG; $n = 4$ for HFD+Sham, and $n = 5$ for HFD+VSG). (**D**) Femoral stiffness, yield load, and maximum load in HFD-fed mice ($n = 8$ for Sham and $n = 7$ for VSG). (**E**) Representative sections from proximal and distal tibiae were stained with H&E and are shown at ×200 magnification. Scale bars, 100 μm. (**F**) Tibial BMAT was visualized and quantified relative to total bone volume within the indicated regions ($n = 5$ for NCD+Sham, $n = 6$ for NCD+VSG, $n = 4$ for HFD+Sham, and $n = 5$ for HFD+VSG). Growth plate (G/P) to tibia/fibula junction (T/F J). Distal tibia is T/F J to distal end. Box and whisker plots show a central median line, boxed 25th and 75th quartiles and the whiskers mark the range. Differences between treatments were evaluated by 1-way ANOVA with Tukey's multiple comparisons test (**A**–**D** and **F**). P values in panels were adjusted across the experiment for multiple testing using limma package in R with FDR method. *Statistical difference at $P < 0.05$.

ulocyte–colony stimulating factor (G-CSF), which is increased in the circulation of mice and humans after VSG. Indeed, elevation of G-CSF mimics many of the effects of VSG on the marrow niche, and G-CSF is required for VSG to suppress marrow adiposity and to robustly induce circulating neutrophils.

Results

Loss of bone and BMAT with VSG is independent of body weight, diet, and sex. To model the conditions in which bone loss is most commonly observed with VSG in humans, we induced obesity in

male C57BL/6J mice with 8 weeks of high fat diet (HFD) prior to sham or VSG surgery. In addition, we controlled for independent effects of HFD on bone metabolism (19, 20) by returning a subset of mice to a normal chow diet (NCD) after surgery. Whereas VSG decreased body weight and fat mass of HFD-fed animals 8 weeks after surgery (Figure 1A), simply switching mice from HFD to NCD caused a substantial reduction of body weight and fat mass that largely masked potential effects of VSG within this treatment group (Figure 1A). Although effects of VSG on body weight and fat mass were dependent on diet, VSG caused a consistent loss of tra-
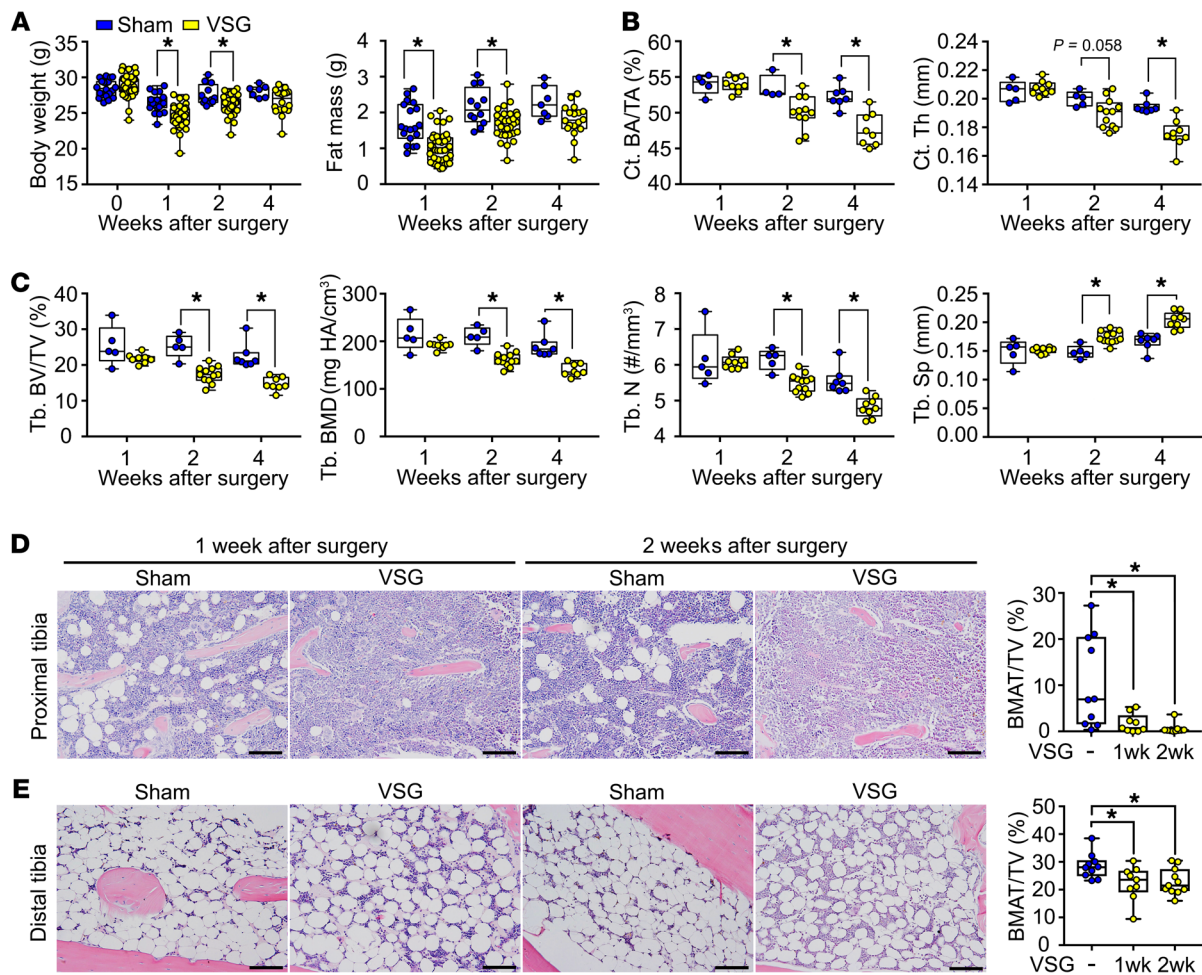
Figure 2. VSG causes rapid loss of bone and BMAT in lean mice. Male mice on a NCD received sham or VSG surgery at 12 weeks of age and were euthanized 1, 2, or 4 weeks later. (**A**) Body weight and fat mass were determined at indicated times (n = 20 for Sham and n = 40 for VSG at 1 week; n = 12 for Sham and n = 30 for VSG at 2 weeks; n = 7 for Sham and n = 18 for VSG at 4 weeks). (**B**) Ct. BA/TA and Ct. Th were measured by μCT. (**C**) Tb. BV/TV, Tb. BMD, Tb. N, and Tb. Sp were also determined (n = 5 for Sham and n = 9 for VSG at 1 week; n = 5 for Sham and n = 12 for VSG at 2 weeks; n = 7 for Sham and n = 8 for VSG at 4 weeks). Representative sections from proximal (**D**) and distal (**E**) tibiae 1 or 2 weeks after surgery were stained with H&E and are shown at ×200 magnification. Scale bars, 100 μm. Decalcified tibiae were stained with osmium tetroxide and volume of BMAT determined for both locations relative to total bone volume (n = 10 for Sham; n = 9 for VSG at 1 week and n = 11 for VSG at 2 weeks). *Statistical difference at $P < 0.05$ by 2-way ANOVA with Sidak's multiple comparisons test (**A**–**C**) and 1-way ANOVA with Tukey's multiple comparisons test (**D** and **E**). P values across **A** to **C** were adjusted for multiple testing using limma package in R with FDR method.

becular and cortical bone in both NCD and HFD groups (Figure 1, B and C). Specifically, VSG mice had decreased trabecular bone volume fraction (Tb. BV/TV), trabecular bone mineral density (Tb. BMD), and trabecular number (Tb. N), whereas spacing between trabeculi was increased (Tb. Sp) (Figure 1B). In addition, cortical area (Ct. BA/TA) and thickness (Ct. Th) were reduced by VSG (Figure 1C). Although mechanical unloading of bone with weight loss is commonly thought to decrease bone mass (21), we did not observe a correlation between body weight and mid-tibial Ct. BA/TA or with Tb. BV/TV (Supplemental Figure 1A; supplemental material available online with this article; https://doi.org/10.1172/JCI126173DS1). Next, we evaluated mechanical properties of bone using a 4-point bending assay and observed that VSG reduces stiffness and maximum load of femurs (Figure 1D), which indicates that bones from VSG mice not only have reduced mass, but are weaker and thus are at higher risk for bone fracture.

Counter to the commonly observed inverse relationship between bone mass and marrow adiposity (16), VSG causes almost complete loss of 'regulated' BMAT in proximal tibia (growth plate to tibia/fibular junction; ref. 22), and about ~30% depletion of 'constitutive' BMAT in distal tibia (Figure 1, E and F; ref. 22). Interestingly, there is a strong positive correlation between distal tibial BMAT and cortical bone mass, but not with gonadal white adipose tissue (gWAT), suggesting that VSG regulates the bone marrow niche independently of effects on adiposity (Supplemental Figure 1B). VSG of female mice causes almost identical effects to those observed in male mice on body weight, fat mass, cortical bone mass, and BMAT. However, loss of trabecular bone with VSG is milder in female mice, and a moderate correlation between body weight and cortical bone mass is observed (Supplemental Figure 1, C–H). To investigate the potential roles of estrogen and body weight in the VSG-induced bone loss, ovariec-
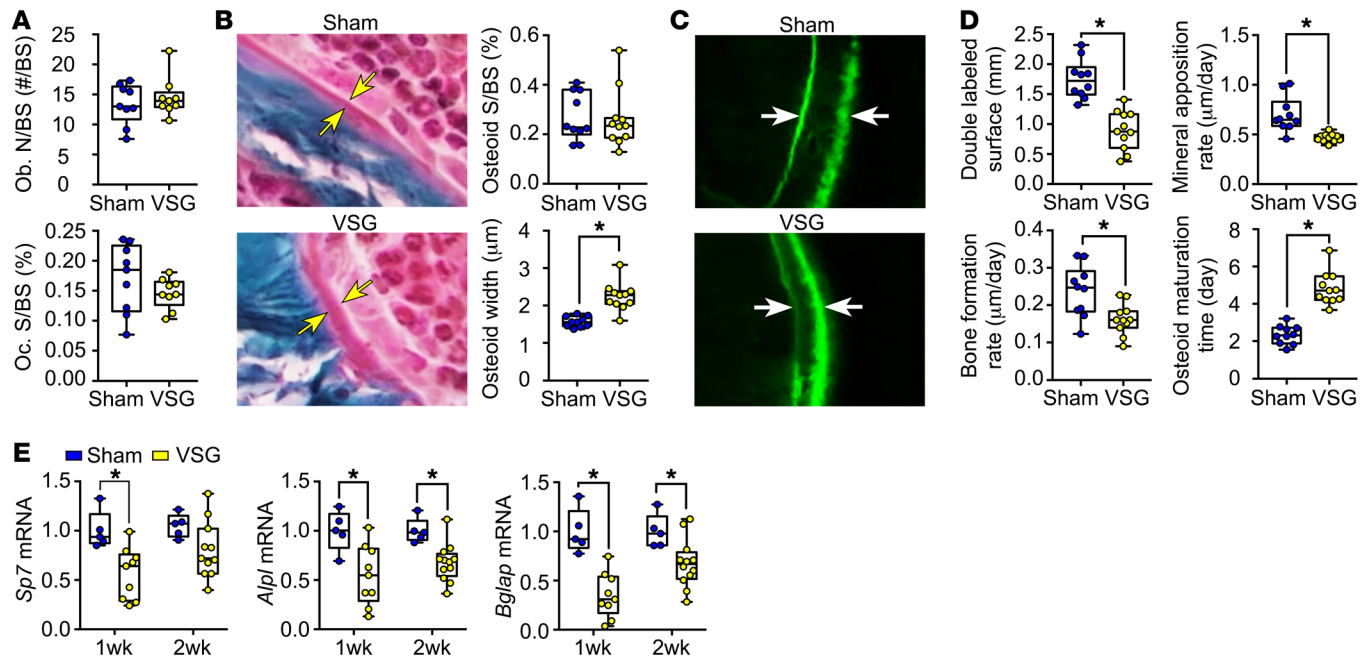
Figure 3. Loss of bone after VSG is due to decreased bone formation and impaired mineralization. Male mice on a NCD received either sham or VSG surgery at 12 weeks of age and were euthanized 2 weeks later. Mice were intraperitoneally injected with calcein (20 mg/kg) 9 and 2 days prior to euthanasia. (**A**) Tibial bone surface (BS) and osteoblast number (Ob. N) were determined on H&E-stained decalcified sections and calculated by Bioquant software. Tibial osteoclast surface (Oc. S) was determined from decalcified TRAP-stained sections and normalized by bone surface (*n* = 9 for each group). (**B**) Undecalcified femurs were embedded in plastic, sectioned, and stained with Masson Trichrome to calculate osteoid surface (S)/bone surface (BS) and osteoid width. Arrows indicate the borders of osteoid surface (*n* = 10 for Sham and *n* = 11 for VSG). (**C**) Calcein-labeled mineralized femurs were sectioned and fluorescence was visualized. Distance between calcein incorporation into mineralized matrix is shown by arrows. (**D**) Analyses of fluorescent double-labeled surface was used to calculate bone formation rate, mineral apposition rate, and osteoid maturation time using Bioquant software (*n* = 10 for Sham and *n* = 11 for VSG). (**E**) Expression of *Sp7*, *Alpl*, and *Bglap* mRNAs from whole femur tissue was analyzed by qPCR and normalized by the expression of the geometric mean of housekeeping genes *Hprt*, *Rpl32A*, and *Tbp* (*n* = 5 for Sham and *n* = 9 for VSG at 1 week; *n* = 5 for Sham and *n* = 12 for VSG at 2 weeks). *Statistical difference for indicated comparisons at $P < 0.05$ by 2-sample *t* test (**A**, **B**, and **D**) and 2-way ANOVA with Sidak's multiple comparisons test (**E**). *P* values across **A** to **D** were adjusted for multiple testing using limma package in R with FDR method.

tomized (OVX) mice received either sham or VSG, and tibial bone variables were determined 8 weeks after surgery. VSG caused a robust loss of Ct. BA/TA and Ct. Th in OVX female mice (Supplemental Figure 1I). Although VSG did not further decrease Tb. BV/TV or Tb. BMD, the basal trabecular bone mass was greatly diminished by OVX and further loss might not have been possible (Supplemental Figure 1J). Importantly, the changes in cortical bone mass with VSG were independent of changes in body weights after ovariectomy.

Because production and secretion of gut peptides are often changed by VSG, and glucagon-like peptide 1R (GLP-1R) and GLP2 peptides have been linked to bone resorption and formation (23, 24), we also examined impact of these alleles on effects of VSG. We observed that effects of VSG on bone mass and BMAT were still observed in mice lacking proglucagon (the gene that encodes GLPs; *Gcg*$^{-/-}$) or glucagon-like peptide-2 receptor (*Glp2r*$^{-/-}$), or in *Gcg*$^{-/-}$ mice in which the locus is reactivated in intestine to restore plasma GLP-1 concentrations (Supplemental Figure 2, Supplemental Figure 3). Effects on loss of bone and BMAT in *Glp2r*$^{-/-}$ mice are independent of food intake, since pair-feeding of sham mice to consumption of food by VSG mice did not alter these variables (Supplemental Figure 3). Taken together, these results demonstrate that VSG-induced loss of bone and BMAT is independent of body weight, diet, food intake, sex, *Gcg*, and *Glp2r*.

VSG causes rapid loss of bone and BMAT in both lean and obese mice. To evaluate how rapidly the effects of VSG occur, we evaluated bone endpoints at 1, 2, and 4 weeks after sham or VSG surgery on lean mice exclusively fed a NCD. In this model, VSG causes a transient decrease of body weight 1 and 2 weeks after surgery with a parallel reduction of fat mass (Figure 2A). VSG caused a significant decrease of cortical and trabecular bone mass as early as the second week of surgery, with further loss 4 weeks after surgery. This effect of VSG held true for Ct. BA/TA and Ct. Th., as well as Tb. BV/TV, Tb. BMD, and Tb. N, and increased Tb. Sp (Figure 2, B and C). We also found that loss of proximal and distal tibial BMAT occurred as early as 1 week after surgery (Figure 2, D and E), with effects persisting for at least 8 weeks (Figure 1, E and F). Thus, effects of VSG on loss of BMAT are independent of white adipose tissue since in this lean cohort of mice loss of fat mass was transient (Figure 2A). Next, we evaluated how rapidly VSG influences mice fed a HFD for 8 weeks. Consistent with the well-known benefits of VSG in weight reduction and type 2 diabetes amelioration (5), we observed a significant decrease of body weight and fat mass in the VSG group as early as 1 or 2 weeks after surgery, without change in the lean body mass (Supplemental Figure 4A). Glucose homeostasis was improved 2 and 4 weeks after VSG (Supplemental Figure 4B). Consistent with the observation in mice fed NCD, trabecular bone loss was observed 2 weeks after surgery
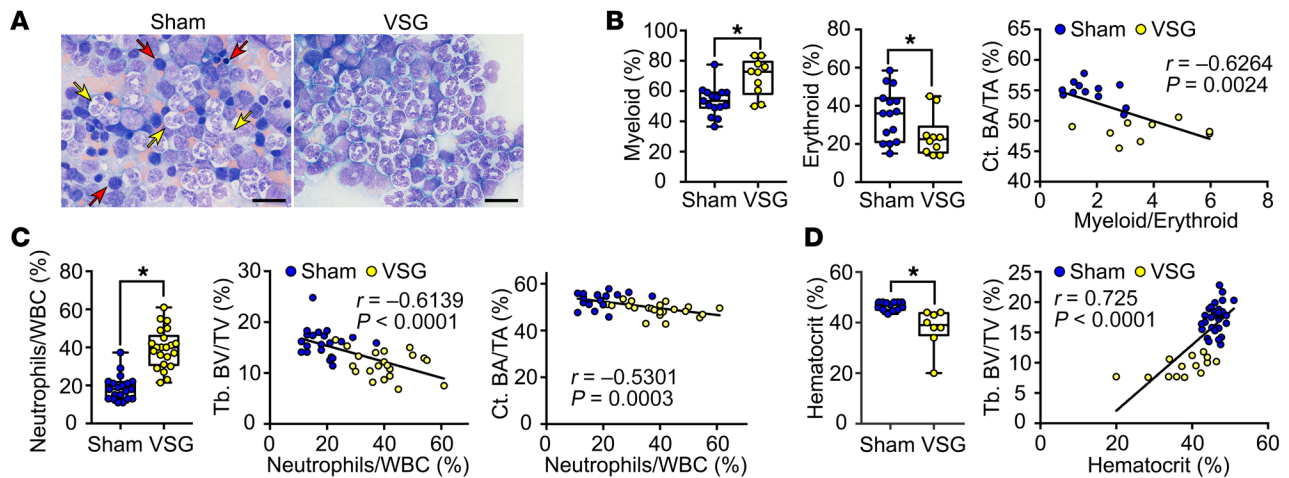
Figure 4. Bone mass after VSG is inversely correlated with myeloid cell expansion. Male mice at 4 weeks of age were fed a 60% HFD for 8 weeks and then received either sham or VSG surgery. Mice remained on a HFD until euthanasia 8 weeks after surgery. (**A**) Wright-Giemsa staining was performed on a femoral bone marrow touch preparation. Representative pictures at ×1000 magnification are shown. Scale bars, 20 μm. Yellow arrows show neutrophils and their myeloid precursors; red arrows show erythroid cells. (**B**) Blind counting of myeloid and erythroid cells was performed by a board-certified pathologist. Linear regression on the relationship between myeloid/erythroid cell ratio and Ct. BA/TA was performed ($n = 15$ for Sham and $n = 10$ for VSG). (**C**) Circulating proportion of neutrophils versus total white blood cells (WBCs) was calculated after performing a CBC. Linear correlations between neutrophil proportion and Tb. BV/TV or Ct. BA/TA are shown ($n = 20$ for Sham and $n = 22$ for VSG). (**D**) Hematocrit was calculated from the CBC. Linear regression demonstrates the positive correlation between hematocrit and Tb. BV/TV ($n = 28$ for Sham and $n = 14$ for VSG). *Statistical difference for indicated comparisons at $P < 0.05$ by 2-sample t test (**B**–**D**).

and was decreased further by 4 weeks (Supplemental Figure 4C), whereas cortical bone loss in obese mice was not observed until 4 weeks after surgery (Supplemental Figure 4D). Circulating bone turnover markers TRACP5b and CTX-1 were significantly higher 4 weeks after surgery in these obese mice (Supplemental Figure 4E), which is consistent with circulating turnover markers in obese VSG patients (25, 26). Effects of VSG on proximal and distal tibial BMATs were also very rapid, with loss observed 2 weeks after surgery (Supplemental Figure 4F).

Loss of bone after VSG is due to decreased bone formation and impaired mineralization. Since cortical and trabecular bone losses are first observed 2 weeks after VSG in both lean and obese mice, we decided this time point would be the optimal period to use histomorphometry to evaluate mechanisms by which VSG influences bone mass. In our analyses of bones from lean mice, VSG does not appear to alter development or turnover of bone cells because osteoblast number and osteoclast surface were unchanged by VSG at this time point (Figure 3A). We then explored whether bone loss might be secondary to elevated bone resorption. This hypothesis is supported by an increase in the circulating marker of osteoclast number, tartrate-resistant acid phosphatase 5b (TRACP5b), which is increased robustly 1 and 2 weeks after surgery and remains elevated compared with sham 4 weeks after surgery (Supplemental Figure 5A). However, femoral expression of TRACP5 (*Acp5*) and receptor activator of nuclear factor kappa-B (RANK, *Tnfrsf11a*) mRNAs were not different 1 week after surgery (Supplemental Figure 5A). This tenet is also supported by our observation of a protective effect from alendronate (AL), an inhibitor of osteoclast function (27), that decreased osteoclast number and surface and blocked the cortical and trabecular bone loss with VSG (Supplemental Figure 5, B–D). On the other hand, elevated bone resorption was not supported in these lean mice by changes in

circulating C-terminal telopeptide of type 1 collagen (CTX-1) and RANK ligand (RANKL; Supplemental Figure 5E). Thus, we looked further into whether bone formation might be impaired by VSG. Although osteoid surface was not statistically altered, the width of the osteoid seam was significantly increased in VSG mice (Figure 3B), suggesting a possible mineralization defect. We ruled out a causative effect through altered calcium homeostasis since serum parathyroid hormone, calcium, vitamin D, and phosphate concentrations were not influenced by VSG or by alendronate treatment (Supplemental Figure 5F).

To further explore altered bone formation as a mechanism, dynamic histomorphometry was performed after injections of calcein given 9 and 2 days prior to euthanasia (Figure 3C). Importantly, 2 weeks after VSG, double-labeled bone surface, bone formation rate, and mineral apposition rate (MAR) were all decreased in VSG mice, whereas the osteoid maturation time was extended (Figure 3D). Furthermore, genes associated with osteoblast differentiation and activity, including osterix (*Sp7*), alkaline phosphatase (*Alpl*), and osteocalcin (*Bglap*), were suppressed as early as the first week after VSG (Figure 3E). However, expression of runt-related transcription factor 2 (*Runx2*) and osteopontin (*Spp1*) mRNAs were unchanged by VSG (Supplemental Figure 5G). One possible mediator of VSG effects is adrenocorticotropic hormone (ACTH), which promotes osteoblast differentiation as well as the osteoclast differentiation cytokine, receptor activator of nuclear factor kappa-B ligand (RANKL) (28). Whereas there was a trend toward decreasing circulating concentrations of ACTH early after surgery, ACTH is unlikely to play an intermediary role since it returned to baseline 4 weeks after VSG (Supplemental Figure 5H). Although further experiments will be required to clarify whether osteoclast activity is important for loss of bone with VSG, our data strongly support a model in which bone formation and mineralization are impaired by VSG.
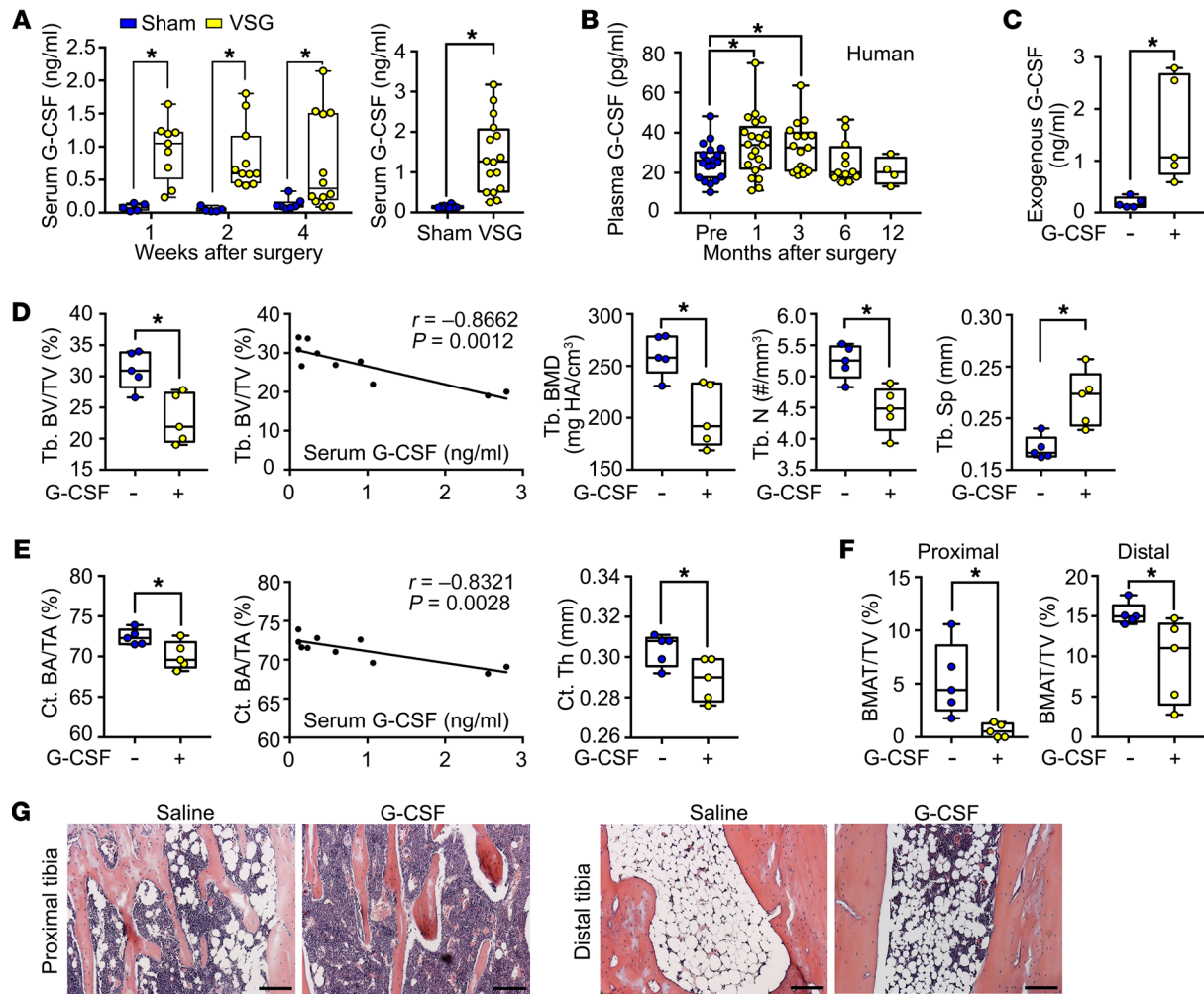
Figure 5. VSG in mice and humans rapidly increases circulating G-CSF, which in mice is sufficient to cause loss of bone and BMAT. (**A**) Circulating G-CSF levels in male C57BL/6J mice were measured at 1, 2, 4, and 8 weeks (right panel) after sham or VSG surgery (Sham, *n* = 5 and VSG, *n* = 9 at 1 week; Sham, *n* = 5 and VSG, *n* = 11 at 2 weeks; Sham, *n* = 7 and VSG, *n* = 12 at 4 weeks; Sham, *n* = 10 and VSG, *n* = 16 at 8 weeks). (**B**) Female young patients underwent VSG surgery. Circulating G-CSF concentrations before (*n* = 22) and at 1 (*n* = 22), 3 (*n* = 17), 6 (*n* = 12), and 12 (*n* = 4) months after surgery. (**C–G**) C3H/HeJ mice at 12 weeks of age were implanted with osmotic minipumps containing saline (–) or recombinant murine G-CSF (+) (3 μg/mouse). Animals were sacrificed 4 weeks after implantation (*n* = 5 for each group). (**C**) Circulating G-CSF concentrations at 4 weeks. (**D**) Tibial trabecular characteristics including Tb. BV/TV, Tb. BMD, Tb. N, and Tb. Sp. The inverse correlation between Tb. BV/TV and circulating G-CSF concentrations is shown. (**E**) Ct. BA/TA and Ct. Th were measured. Linear regression reveals the inverse correlation between Ct. BA/TA and circulating G-CSF concentrations. (**F**) Proximal and distal tibial BMAT volume was determined by osmium staining and μCT. (**G**) Representative H&E-stained sections from proximal and distal tibiae with ×200 magnification are shown. Scale bars, 100 μm. *Statistical difference for indicated comparisons at *P* < 0.05 by 2-way ANOVA with Sidak's multiple comparisons test (**A**), Wilcoxon matched-pair signed rank test (**B**), and 2-sample *t* test (**C–F**). *P* values across **C** to **F** were adjusted for multiple testing using limma package in R with FDR method.

Bone mass after VSG is inversely correlated with myeloid cell expansion. Bone is a closed physical space, thus the rapid depletion of bone mass and BMAT by VSG is likely associated with expansion of other cell types. Based on the morphology of cells within Figure 1E, we hypothesized that VSG causes expansion of hematopoietic cellularity. We collected femurs from the mice with sham or VSG surgeries for 8 weeks and performed differential counts on Wright-Giemsa–stained bone marrow touch preparations in a blinded manner. The populations included cells of myeloid, erythroid, lymphocyte, monocyte, and eosinophil lineages. We found that the proportion of myeloid cells was increased, whereas the proportion of erythroid cells was decreased by VSG (Figure 4, A and B). Moreover, the ratio of myeloid versus erythroid cellularity was inversely correlated with Ct. BA/TA (Figure 4B). Consistent with the expansion of myeloid cells in bone marrow, the proportion of circulating neutrophils was increased by VSG, and was inversely correlated with Tb. BV/TV and Ct. BA/TA (Figure 4C). We considered whether wound-healing or inflammation after VSG caused the increase of neutrophils; however, the following observations did not support this hypothesis. The transient increase of interleukin 6 (IL-6) and total white blood cell (WBC) number 1 week after VSG returned to baseline levels by 2 weeks, and circulating tumor necrosis factor α (TNF-α) was not influence by VSG surgery (Supplemental Figure 6A). Consistent with these observations, Ridelman et al. showed that circulating biomarkers, including monocyte chemo-
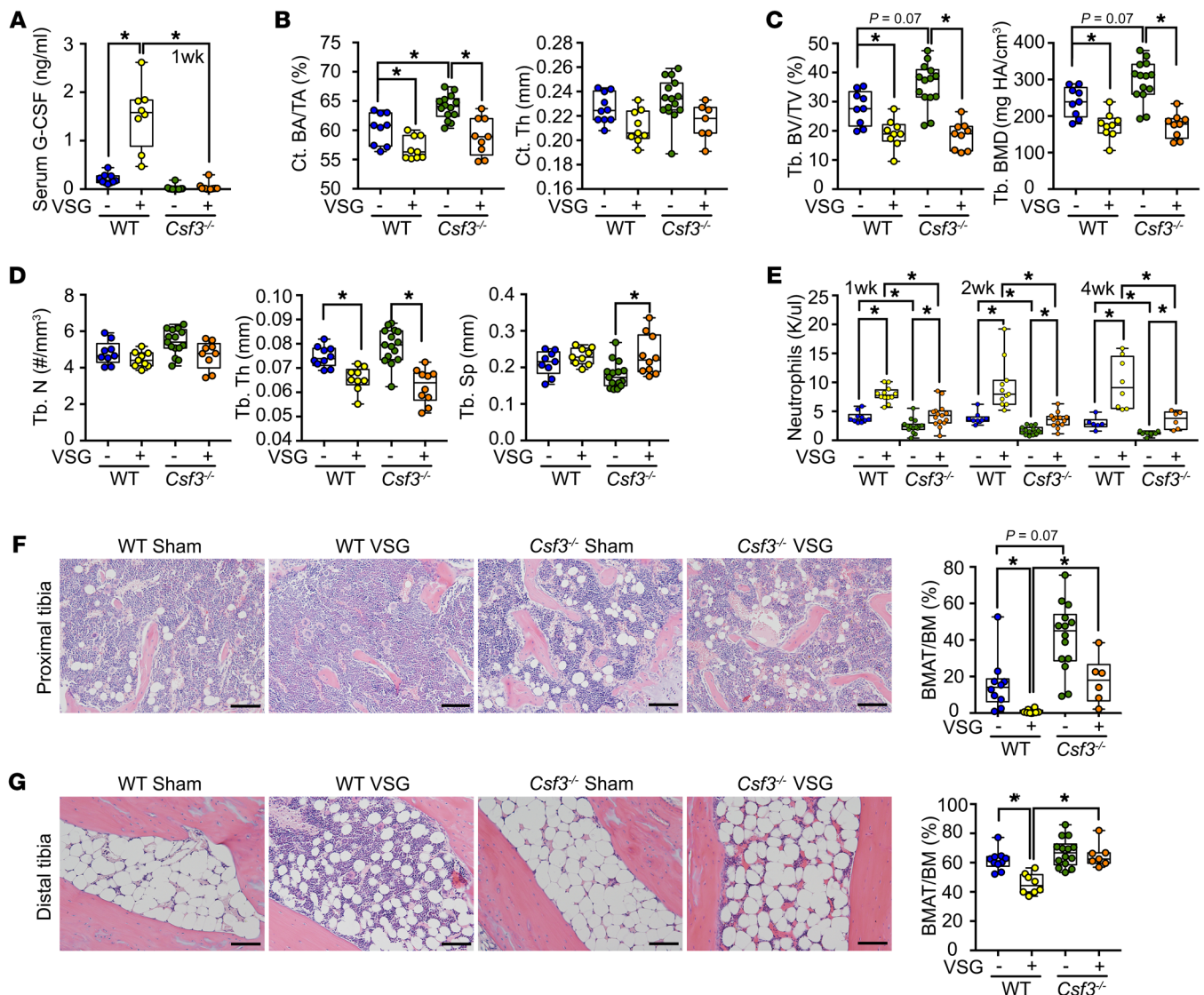
Figure 6. G-CSF is not required for VSG-induced bone loss, but is necessary for complete effects on circulating neutrophils and BMAT. Female *Csf3*⁻/⁻ mice and their littermates (WT) at 12 weeks of age received a sham (–) or VSG (+) surgery and were euthanized 4 weeks later. (**A**) Circulating G-CSF concentrations 1 week after surgery. (**B**) Ct. BA/TA and Ct. Th were measured by μCT. (**C–D**) Tb. BV/TV, Tb. BMD, Tb. N, Tb. Th, and Tb. Sp were determined (**A–D**: n = 9 for WT+Sham; n = 9 for WT+VSG; n = 14 for *Csf3*⁻/⁻+Sham and n = 9 for *Csf3*⁻/⁻+VSG). (**E**) Circulating neutrophil number at the indicated times after surgery (n = 10 for WT+Sham; n = 12 for WT+VSG; n = 15 for *Csf3*⁻/⁻+ Sham and n = 15 for *Csf3*⁻/⁻+VSG at 1 week; n = 9 for WT+Sham; n = 11 for WT+VSG; n = 15 for *Csf3*⁻/⁻+Sham, and n = 13 for *Csf3*⁻/⁻+VSG at 2 weeks; n = 6 for WT+Sham; n = 8 for WT+VSG; n = 10 for *Csf3*⁻/⁻+Sham, and n = 7 for *Csf3*⁻/⁻+VSG at 4 weeks). Representative H&E sections from (**F**) proximal and (**G**) distal tibiae at ×200 magnification are shown (n = 10 for WT+Sham; n = 8 for WT+VSG; n = 14 for *Csf3*⁻/⁻+Sham, and n = 7 for *Csf3*⁻/⁻+VSG). Scale bars, 100 μm. Decalcified tibiae were stained with osmium tetroxide and BMAT volume determined by μCT and normalized by bone marrow (BM) volume. *Statistical difference for indicated comparisons at $P < 0.05$ by 1-way ANOVA with Tukey's multiple comparisons test (**A–D** and **F–G**) and 2-way ANOVA with Sidak's multiple comparisons test (**E**). P values across the experiment were adjusted for multiple testing using limma package in R with FDR method.

attractant protein-1 (MCP-1/CCL2), keratinocyte chemoattractant (KC), and TNF-α, were unchanged by VSG in mice fed NCD or HFD diet (29). Furthermore, the neutrophils persisted at higher levels for at least 8 weeks after VSG (Figure 4C; Supplemental Figure 6B), whereas the monocyte and lymphocyte populations were not different (Supplemental Figure 6, C and D), suggesting that a neutrophil-stimulating factor might be the cause.

Consistent with the decrease of erythroid cellularity in bone marrow, the hematocrit of VSG mice was reduced and was positively correlated with Tb. BV/TV (Figure 4D). One possible mech-

anism for anemia is vitamin B₁₂ deficiency since absorption of this nutrient is dependent on intrinsic factor, which is produced by the stomach. Surprisingly, we do not detect vitamin B₁₂ deficiency 4 weeks after VSG (Supplemental Figure 6E). Whereas a decrease of red blood cell number and hemoglobin was observed 1 week after VSG, microcytic anemia was not observed until 2 weeks after VSG (Supplemental Figure 6F). Although circulating iron concentrations were unchanged through 4 weeks after VSG (Supplemental Figure 6G), further experiments will be required to establish the mechanistic basis underlying the anemia.

We next tested whether the VSG surgical procedure or wound healing process itself might cause a nonspecific immunological reaction resulting in effects on bone mass and the marrow niche. Thus, we performed an additional pilot cohort that included a so-called staple sham group, which involved stomach incision and suturing, and staples onto the stomach, but without decreasing the stomach volume (Supplemental Figure 6, H and I). The staple sham surgery did not influence cortical or trabecular bone mass, nor did it influence BMAT in proximal and distal tibia. These data indicate that the bone and BMAT loss caused by VSG is not associated with the surgical procedure but is instead related to the decrease of stomach volume.

VSG in mice and young female patients rapidly increases circulating G-CSF, which in mice is sufficient to cause loss of bone and BMAT. In our consideration of possible mechanisms by which VSG influences the bone marrow niche, G-CSF caught our attention because of its ability to inhibit osteoblast function and impair endosteal bone formation (30), to stimulate myelopoiesis and to increase circulating neutrophils (31, 32). Consistent with this notion, we observed that circulating G-CSF concentrations are rapidly increased in mice during the week following VSG, and remain elevated for at least 8 weeks (Figure 5A). To explore whether G-CSF is also regulated by VSG in humans, we obtained plasma from young obese female patients (17–20 years) before and at various times after surgery. G-CSF in circulation was transiently increased 1 and 3 months after surgery, with a return to baseline levels at 6 and 12 months (Figure 5B). Unfortunately, bone mass measurements were not made on this patient population.

Inflammatory cytokines are a well-known stimulus to increase production of G-CSF (33, 34). To investigate whether G-CSF elevation might be caused by an inflammatory response to infection, we treated HFD-fed mice with antibiotics for postsurgical weeks 1 through 4 and found that serum G-CSF concentrations were still elevated by VSG. Importantly, circulating bone turnover markers TRACP5b and CTX-1 (Supplemental Figure 7, A and B) were also higher, indicating that effects of VSG on G-CSF and bone loss are independent of inflammation.

To test whether elevated G-CSF is sufficient to mimic effects of VSG on the bone marrow niche, we used mouse models in which we increased circulating concentrations of G-CSF by overexpression of its gene, *Csf3*, or by implantation of an osmotic mini-pump that releases exogenous G-CSF. The C3H/HeJ mouse strain was chosen as an ideal model because bone mass and BMAT are higher than C57BL/6J at baseline (22). First, we injected AAV-*Csf3* via tail vein to overexpress G-CSF and AAV-*Egfp* was injected as a control. Viral delivery of *Csf3* caused a dramatic increase of circulating G-CSF in the weeks following infection (Supplemental Figure 7C) and decreased cortical and trabecular bone mass in a manner dependent on G-CSF concentration (Supplemental Figure 7, D and E). Moreover, at these supraphysiological concentrations of G-CSF, bone marrow adipocytes were almost completely depleted from BMAT depots of the proximal and distal tibia (Supplemental Figure 7F). As expected (32, 35), AAV-*Csf3* caused increased circulating neutrophils and splenomegaly (Supplemental Figure 7G), which was also observed after VSG (Supplemental Figure 7H). High circulating G-CSF concentrations were well-tolerated, and differences in body weight, random blood glucose levels, and liver

weight were not observed (Supplemental Figure 7I). In summary, ectopic delivery of *Csf3* caused high G-CSF concentrations, which were sufficient to closely mirror effects of VSG on bone mass, BMAT, and hematopoiesis.

To determine whether the elevated concentrations of G-CSF observed after VSG are also sufficient to influence the bone and marrow niche, we implanted osmotic mini-pumps filled with saline or G-CSF (3 μg/mouse) for 4 weeks. Circulating G-CSF concentrations varied from 0.6 ng/ml to 2.8 ng/ml (Figure 5C), which is within the range found after VSG in mice (Figure 5A). Importantly, these concentrations of exogenous G-CSF were sufficient to reduce trabecular bone mass in a concentration-dependent manner, with decreases in Tb. BV/TV, Tb. BMD, and Tb. N, and increases in Tb. Sp (Figure 5D). Similar concentration-dependent results were observed for loss of Ct. BA/TA and Ct. Th (Figure 5E). Although not altered by VSG, histological analyses revealed that G-CSF administration increased osteoclast and osteoblast number per bone surface (Supplemental Figure 7J). Consistent with all other VSG cohorts of lean and obese mice, TRACP5b was increased in those mice with the highest circulating G-CSF, whereas the CTX-1 was largely unchanged in response to G-CSF administration (Supplemental Figure 7K). Finally, we also observed that exogenous G-CSF decreased BMAT in both proximal and distal tibia (Figure 5, F and G). Taken together, these data provide strong evidence that induction of G-CSF by VSG is sufficient to mediate many of the VSG effects on the bone and marrow niche.

VSG causes bone loss through mechanisms independent of G-CSF. To determine whether G-CSF is required for effects of VSG, we performed sham or VSG surgeries on global G-CSF (*Csf3*) knockout (*Csf3*⁻/⁻) mice and their wild-type (WT) littermates. Whereas VSG increased circulating G-CSF in WT animals for postsurgical weeks 1 through 4, plasma concentrations of G-CSF were barely detectable in knockout mice under any condition (Figure 6A; Supplemental Figure 8A). As expected from our prior findings (Figure 1, Figure 2), VSG did not alter body weight in NCD WT mice, and this observation held true for *Csf3*⁻/⁻ mice (Supplemental Figure 8B). Consistent with the bone loss induced by G-CSF overexpression or exogenous administration, knockout of endogenous *Csf3* increases the Ct. BA/TA (Figure 6B), and tended to increase Tb. BV/TV and Tb. BMD relative to WT animals (Figure 6C), suggesting that baseline bone mass is set, in part, by circulating G-CSF concentrations. However, deficiency of *Csf3* did not prevent loss of cortical or trabecular bone induced by VSG (Figure 6, B–D), suggesting that mechanisms independent of G-CSF are also able to mediate bone loss.

G-CSF is partially required for VSG to increase circulating neutrophils and deplete BMAT. We next evaluated whether G-CSF is required for effects of VSG on other aspects of the bone marrow niche, including hematopoiesis and marrow adiposity. As expected, VSG stimulates a robust increase in circulating neutrophils at 1, 2, and 4 weeks after surgery in WT mice (Figure 6E). Whereas the baseline number of neutrophils is lower in *Csf3*⁻/⁻ mice, VSG still increases circulating neutrophils to approximately 30% of controls at each of these time points, suggesting that the induction of myelopoiesis by VSG partially requires G-CSF (Figure 6E). Although anemia was not as severe in this cohort, perhaps because of mixed genetic background, both WT and *Csf3*⁻/⁻ mice had reductions of mean corpuscular hemoglobin, with the decrease

being greater in the *Csf3*−/− mice (Supplemental Figure 8C). Finally, we evaluated the effects of VSG on BMAT. Similar to the increase observed in cortical and trabecular bone mass, *Csf3* deficiency is associated with a trend of induction in regulated BMAT of proximal tibia (Figure 6F). Whereas VSG almost completely depleted BMAT in proximal tibia of WT mice, VSG only reduced BMAT in proximal tibia of *Csf3*−/− mice by about 50% (Figure 6F). Importantly, VSG did not cause any loss of constitutive BMAT of distal tibia in *Csf3*−/− mice (Figure 6G), consistent with G-CSF playing an intermediary role in this process. Taken together, these data indicate that endogenous G-CSF, in addition to its well-known effects on myelopoiesis, impairs development of bone marrow adipocytes and accrual of bone. Although G-CSF is not required for VSG to stimulate bone loss, endogenous G-CSF is required for a subset of VSG effects on the bone marrow niche, including full expansion of circulating neutrophils and depletion of BMAT.

Discussion

Bariatric surgery causes significant and consistent bone loss in both mice and humans, although the mechanisms have not been clearly delineated (8, 36). Importantly, bone loss after bariatric surgery is independent of body weight loss and circulating calcium or vitamin D concentrations (37). However, clues to the mechanisms of bone loss may come from other effects of VSG on the bone marrow niche, specifically the opposing effects on myelopoiesis and marrow adipocytes. In this study, we identified G-CSF as one potential factor to cause these changes in the bone marrow niche in response to VSG. Intriguingly, rats are not an ideal animal model in this regard because they do not exhibit bone loss after VSG (15). Human studies have focused primarily on Roux-en-Y gastric bypass (RYGB), although there has been limited work on VSG that indicated whole body and hip bone mineral density decline as early as 3 months after surgery (38, 39). Bredella et al. also observed a global decline of BMD of spine, hip, and femoral neck after 12 months (26). Although shorter intervals have not been carefully evaluated in humans, we observed that VSG caused loss of cortical and trabecular bone in mice generally as early as 2 or 4 weeks after surgery.

Early work on bone loss in humans after bariatric surgeries focused on calcium and vitamin D malabsorption (37). Patients routinely receive calcium and vitamin D supplements after bariatric surgeries, and circulating levels of calcium, 25(OH)-vitamin D, and parathyroid hormone are not influenced by bariatric surgeries (26, 40). As with humans, our work in mice also dissociates bone loss after VSG from those variables. We observed that circulating concentrations of calcium, parathyroid hormone, and vitamin D were unaltered in the 4 weeks after surgery, even in the absence of supplementation. In addition, treatment of mice with alendronate to block bone reabsorption did not cause a decline in circulating calcium, indicating that calcium at these early time points is not limiting. The unloading of bones with weight loss has also been investigated as a potential mechanism in humans (21). Again, our work in mice corroborates what was found in patients, that is, that bone loss after VSG is independent of weight loss.

Clinical studies consistently report that markers of bone turnover (i.e., CTX-1) and formation (i.e., P1NP) are increased in patients after bariatric surgeries, including VSG (39). We sim-

ilarly observed that TRACP5b (circulating osteoclast marker) was induced and P1NP was higher 4 weeks after VSG in mice (Supplemental Figure 5I), although induction of CTX-1 was not observed during the 4 weeks after surgery in lean mice. However, histomorphometric analyses 2 weeks after surgery, the earliest point of bone loss, revealed that VSG did not alter osteoblast number nor osteoclast surface in this time frame, but rather reduced the bone formation and mineral apposition rate while it increased mineralization lag time. Consistent with reduced osteoblast function, expression of osteoblast genes such as *Sp7*, *Alpl*, and *Bglap* are suppressed by VSG as early as 1 week after surgery. Taken together, these data suggest VSG causes an osteoblast defect that leads to impaired mineralization and rapid uncoupling in bone turnover.

In our mouse model after surgery, we also observed profound effects of VSG on the bone marrow niche, where the proportion of neutrophils and their precursors was increased and that of erythroid cells was decreased. Increased marrow myelopoiesis translated to a high number and proportion of circulating neutrophils, with little or no differences in monocytes and lymphocytes. We ruled out the possibility of a nonspecific inflammatory or wound-healing response caused by the surgical procedure, per se, suggesting that a myeloid/neutrophil-stimulating factor is increased by VSG. The clinical literature about effects of bariatric surgery on hematopoiesis is limited. Several reports show a decrease of total WBC and neutrophil numbers 1 year after RYGB (41–43), while there is one report suggesting that WBC and neutrophil numbers decreased 30 days after VSG (44). Although we observed a decrease of WBC and neutrophil numbers in the lean mice after VSG over time, the proportion of neutrophils is persistently higher than in sham mice. Other effects of bariatric surgery on hematopoiesis are suggested by anemia, which occurs in about 5% of VSG patients, and at higher rates in RYGB patients (18). Anemia is also consistently observed after VSG in mice. Despite unchanged circulating vitamin B₁₂ and iron concentrations after VSG, microcytic anemia developed 2 to 4 weeks after surgery in mice.

Across a wide range of physiological and pathological states, there is often an inverse relationship between bone mass and marrow adiposity (16); however, recent work suggests that this relationship is correlational rather than causal (22). Of particular interest to us was whether expansion of BMAT would occur with VSG, as it does with calorie restriction. Counter to our original hypothesis, VSG depletes the proximal regulated BMAT of the tibia, and even causes an approximate 30% loss of the constitutive BMAT found in the distal tibia. The decrease in BMAT volume is largely due to a decrease in the number of marrow adipocytes, with little difference in size of those constitutive marrow adipocytes remaining weeks after VSG. In patients, the effects of bariatric surgery on BMAT are not clear. Bredella et al. detected no change in BMAT in patients undergoing RYGB, but an increase in BMAT in VSG patients 12 months after surgeries (26). On the other hand, Kim et al. and Schafer et al. observed a reduction of BMAT in diabetic subjects at 6 months after RYGB (45, 46).

Several etiological factors have been considered as mediators of bone loss after bariatric surgery, including gut hormones (i.e., PYY, ghrelin, GLPs), adipokines (i.e., adiponectin and leptin), and gonadal hormones (8). However, the evidence to support any of these alone or in combination as primary mech-

anisms of bone loss is scant. Based on our observations with VSG, we hypothesized that the cytokine G-CSF might play an intermediary role since G-CSF had previously been shown to decrease bone formation (30), increase bone resorption (47), and strongly stimulate expansion of neutrophils and their precursors (31, 32). In mice, we observed induction of circulating G-CSF within 1 week of VSG, and elevated concentrations persisted for at least 8 weeks after surgery. In our patient cohorts, we observed a transient induction at 1 and 3 months with a return to baseline at 6 months in a young female cohort, which indicates that G-CSF might contribute to the initial or early stage of VSG-induced bone loss rather than long-term effects. Using 2 gain-of-function approaches, we found that G-CSF alone is sufficient to mimic many of the effects of VSG in mice, including loss of bone and BMAT, expansion of marrow myeloid cellularity, and an increase in circulating neutrophils. One mechanism by which G-CSF likely acts in this context is to increase bone marrow sympathetic drive, which has been associated with bone loss and reduced BMAT in proximal and mid-tibia (47–49). Notably, anemia was not observed, even in mice with very high concentrations of G-CSF. Consistent with these results, *Csf3* knockout mice had increased cortical bone mass, indicating that endogenous G-CSF regulates bone mass even in the absence of VSG. Although G-CSF was not required for VSG to cause bone loss, endogenous G-CSF was necessary for VSG to deplete constitutive BMAT of distal tibia, and appeared to be required for full loss of proximal tibial BMAT after surgery. It is conceivable that the role of endogenous G-CSF in bone loss with VSG is masked by compensatory factors, since a partial increase of neutrophils following surgery is still observed.

Bariatric surgery has been a major advance in the management of both morbid obesity and type 2 diabetes mellitus. Indeed, bariatric surgery is the only approach to cure the latter in nearly 50% of patients (1). However, there are long-term side effects, including loss of bone mass and a greater risk of fracture. Hence, understanding the mechanisms that underlie skeletal effects of bariatric surgery is essential when considering possible preventive measures. The current studies support the use of mice to explore mechanisms by which VSG influences the bone marrow niche. Taken together with our studies in humans, it is likely that G-CSF plays a modulatory role in the skeletal and marrow response to bariatric surgery.

Methods

Subject recruitment and description

Plasma of patients receiving VSG was obtained from the Pediatric Obesity Tissue Repository, Center for Bariatric Research and Innovation, at the Cincinnati Children's Hospital Medical Center. Twenty-two obese female patients with ages 17–20 were recruited. Plasma was collected before surgery and 1, 3, 6, and 12 months after VSG.

Animals

C57BL/6J (Figures 1–4) and C3H/HeJ (Figure 5) mice were from the Jackson Laboratory. G-CSF (*Csf3*) knockout mice (129/SvJ) were donated by Jason M. Shohet from Baylor College of Medicine (50) and we cross-bred these with C57BL/6J mice. Proglucagon knockout

(*Gcg*$^{-/-}$) mice, *Villin 1*-cre mice, and GLP-2 receptor (*Glp2r*$^{-/-}$) knockout mice were as previously reported (51, 52). Mice were housed in a 12-hour light/dark cycle in the Unit for Laboratory Animal Medicine at the University of Michigan, with free access to water. Mice were provided ad libitum access to NCD or HFD (60% calories from fat, D12492; Research Diets), as indicated.

Surgical procedures

Vertical sleeve gastrectomy. Lean and HFD-fed obese C57BL/6J mice were randomly assigned into sham and VSG groups. Sham surgery included opening the abdomen, isolating the stomach, and closing the incision. For the VSG surgery, the lateral 60% of the stomach was resected using an ETS35 stapler (Ethicon Endo-Surgery), leaving a tubular gastric remnant in continuity with the esophagus proximally and the pylorus distally. Mice were fed a liquid diet (Osmolite 1 cal) for the first 4 days after surgery, and thereafter were maintained on NCD or HFD throughout the study. Body weight was monitored weekly for the duration of the experiment. Body composition was assessed via NMR (Echo MRI) prior to and at various time points (1, 2, 4, and 8 weeks) after surgery. Blood was taken from the tail vein or by heart puncture for the complete blood cell (CBC) analysis, and for measurement of serum G-CSF and bone turnover markers.

Ovariectomy. Female 4-week-old mice were fed with a 60% HFD for 7 weeks prior to OVX. After recovering for 5 weeks, VSG or sham surgery was performed on these mice. Each group was then fed NCD or HFD for an additional 8 weeks.

Alendronate treatment. C57BL/6J male mice were fed a NCD until they were 12 weeks old, at which point they received a VSG or sham surgery. Two weeks after surgery, a subgroup of VSG mice was administered intraperitoneal alendronate (300 μg/kg; Sigma-Aldrich) twice per week for 2 weeks.

Antibiotic treatment. C57BL/6J male mice were fed a 60% HFD for 10 weeks before surgery. A combination of ampicillin (1 g/l), neomycin (1 g/l), metronidazole (1 g/l), and vancomycin (0.5 g/l) was included in drinking water from the first week after surgery until euthanasia at week 4. Antibiotic solutions were kept in amber bottles and changed every 2 days.

Osmotic minipump implantation. C3H/HeJ mice were anesthetized with ketamine and xylazine. A 1-cm incision was made in the skin of the back and mice were implanted subcutaneously with an Alzet osmotic minipump (Model 1004) filled with vehicle (saline) or mouse recombination G-CSF (3 μg/mouse; PeproTech) for 28 days. Before implantation, pumps were filled with the test agent and placed in a Petri dish with sterile 0.9% saline at 37°C for at least 4 hours before implantation to prime the pumps.

AAV-Csf3 injection. AAV9-CAG-mCSF3 (AAV-*Csf3*) and AAV9-CAG-eGPF (AAV-*Egfp*) stocks were purchased from Vector Biolabs. Genome copies of AAV-*Csf3* virus (1.5 × 10^{11}) were injected via tail vein, and an equal amount of AAV-*Egfp* was injected into the control group. Animals were euthanized 4 weeks after injection.

Measurement of circulating factors

Circulating G-CSF concentrations were determined with a human or mouse G-CSF quantikine enzyme-linked immunosorbent assay (ELISA; R&D Systems). Mouse RANKL/TNFSF11 ELISA kit was from R&D Systems. Mouse TRACP5b, CTX-1, and P1NP were determined by ELISA (ImmunoDiagnostic Systems). Serum PTH 1-84 (Immutopics, Inc.)

and vitamin B_{12} (Novus Biologicals) concentrations were measured by ELISA kits according to manufacturers' instructions. Serum concentrations of known bone regulators, including adrenocorticotropic hormone (ACTH), interleukin 6 (IL-6), and tumor necrosis factor alpha (TNF-α), were measured by Luminex xMAP assay (Bone Panel). Serum 25(OH)-vitamin D and phosphate concentrations were measured with assay kits from Cayman Chemical. Plasma samples were collected from heparinized blood and used for measurement of total calcium using the Calcium Assay Kit from Cayman Chemical and total circulating iron (Fe^{2+} and Fe^{3+}) using the QuantiChrom Iron Assay Kit (DIFE-250; BioAssay Systems) according to the manufacturers' directions.

Histology and histomorphometry

Tissues were fixed in 10% neutral-buffered formalin for 24 hours. Tibiae were used for microcomputed tomography (μCT) scanning and then decalcified in 14% EDTA for 3 weeks. Paraffin-embedded tissue sections were processed and stained with H&E and tartrate-resistant acid phosphatase (TRAP) as indicated. Following the H&E and TRAP staining on paraffin sections of bone, slides were scanned at ×200 magnification. Static measurements included bone volume fraction, trabecular number and thickness, osteoblast (H&E staining) and osteoclast (TRAP staining) count, and eroded surface. Undecalcified femur was used for plastic sectioning. Mineralized trabecular bone and osteoid (unmineralized trabecular bone) were evaluated with Masson Trichrome Staining. For dynamic studies, calcein (C0857; Sigma-Aldrich) dissolved in 0.02 g/ml sodium bicarbonate with 0.9% saline at 20 mg/kg was injected intraperitoneally 9 and 2 days before sacrifice for quantification of mineral apposition rate (MAR), mineralizing surface to bone surface (MS/BS), and bone formation rate (BFR) in femur. Calculations were made with Bioquant Osteo 2014 software in a blind randomized manner (53, 54).

μCT analysis

Tibiae were placed in a 19-mm diameter specimen holder and scanned over the entire length of the tibiae using a μCT system (μCT100 Scanco Medical). Scan settings were as follows: voxel size 12 μm, 70 kVp, 114 μA, 0.5 mm AL filter, and integration time 500 ms. Density measurements were calibrated to the manufacturer's hydroxyapatite phantom. Analysis was performed using the manufacturer's evaluation software and a threshold of 180 for trabecular bone and 280 for cortical bone.

Marrow fat quantification by osmium tetroxide staining and μCT

After analyses of bone variables, mouse tibiae were decalcified for osmium tetroxide staining using our previously published method (22). In addition, a lower threshold (300 Gy) was used for BMAT quantification in lean mice because density of osmium staining is low due to smaller adipocyte size.

Mechanical testing: 4-point bending

Following μCT scanning, femora were loaded to failure in 4-point bending using a servohydraulic testing machine (MTS 858 MiniBionix). All specimens were kept hydrated in saline-soaked gauze until mechanical testing. In the same mid-diaphyseal region analyzed by μCT, the mid-diaphysis was loaded in 4-point bending with the posterior surface oriented under tension. A custom MATLAB script was used to calculate stiffness, yield load, yield displacement, ultimate load, failure displacement, post-yield displacement, and energy to failure (55).

Wright-Giemsa staining

A drop of blood from tail vein was used for blood smear, and femur was cut in half by razor blade for bone marrow touch preparation. After air drying, slides were stained with Wright-Giemsa stain and differential cell types counted at ×1000 magnification (56).

RNA extraction and quantitative real-time PCR (qPCR)

RNA was extracted from mouse femur after powdering in liquid nitrogen and lysis in RNAStat60 reagent in a precooled Bullet Blender Gold as previously described (49). Quantitative PCR was performed using an Applied Biosystems QuantStudio 3 qPCR machine. Gene expression was calculated based on a cDNA standard curve within each plate and normalized to expression of the geometric mean of housekeeping genes *Hprt*, *Rpl32A*, and *Tbp*.

Statistics

Significant differences between groups were assessed using a 2-sample *t* test or ANOVA with post-tests as appropriate: 1-way ANOVA with Tukey's multiple comparisons test and 2-way ANOVA with Sidak's multiple comparisons test. *P* values in figures were adjusted for multiple testing using limma package in R with FDR method. In Figure 6 and Supplemental Figure 8, 1-way or 2-way ANOVA was performed after $\log_{10}$ transformation of data. Significant differences in circulating factors in human subjects before and after undergoing VSG were assessed using a Wilcoxon matched-pair signed rank test, with comparisons made between baseline and 1, 3, 6, and 12 months after treatment. All analyses were conducted using the GraphPad Prism version 7.0c. Whisker boxes show the 25th and 75th quartiles, with median and range also represented. All other graphic presentations are mean ± SD. For statistical comparisons, a *P* value of less than 0.05 was considered significant.

Study approval

All subjects recruited at Cincinnati Children's Hospital Medical Center provided written informed consent approved by the Cincinnati Children's Institutional Review Board, which reviews research in accordance with applicable federal and state regulations as well as AAHRPP accreditation standards. All procedures for mouse studies were approved by the University of Michigan Committee on the Use and Care of Animals.

Author contributions

ZL, RJS, KS, DAS, CJR and OAM conceived the studies and planned the experimental design. ZL, JH, SSE, CRH, SMC, YS, BSL, KTL, RLS, HM, DPB, SMR, KSK, EB, and CG performed the experiments and analyzed the data. ZL and OAM wrote the manuscript. All other authors edited and approved the final manuscript.

Address correspondence to: Ormond A. MacDougald, Brehm Center, Rm 6313, 1000 Wall Street, Ann Arbor, Michigan 48105, USA. Phone: 734.647.4880; Email: macdouga@umich.edu.

1. Kapeluto J, Tchernof A, Biertho L. Surgery for diabetes: clinical and mechanistic aspects. *Can J Diabetes*. 2017;41(4):392–400.
2. English WJ, DeMaria EJ, Brethauer SA, Mattar SG, Rosenthal RJ, Morton JM. American Society for Metabolic and Bariatric Surgery estimation of metabolic and bariatric procedures performed in the United States in 2016. *Surg Obes Relat Dis*. 2018;14(3):259–263.
3. le Roux CW, Heneghan HM. Bariatric surgery for obesity. *Med Clin North Am*. 2018;102(1):165–182.
4. Hutch CR, Sandoval D. The role of GLP-1 in the metabolic success of bariatric surgery. *Endocrinology*. 2017;158(12):4139–4151.
5. Cummings DE, Rubino F. Metabolic surgery for the treatment of type 2 diabetes in obese individuals. *Diabetologia*. 2018;61(2):257–264.
6. Evers SS, Sandoval DA, Seeley RJ. The physiology and molecular underpinnings of the effects of bariatric surgery on obesity and diabetes. *Annu Rev Physiol*. 2017;79:313–334.
7. Zhang Q, et al. A meta-analysis of the effects of bariatric surgery on fracture risk. *Obes Rev*. 2018;19(5):728–736.
8. Stein EM, Silverberg SJ. Bone loss after bariatric surgery: causes, consequences, and management. *Lancet Diabetes Endocrinol*. 2014;2(2):165–174.
9. Schafer AL, et al. Effects of gastric bypass surgery on bone mass and microarchitecture occur early and particularly impact postmenopausal women. *J Bone Miner Res*. 2018;33(6):975–986.
10. Yu EW, Lee MP, Landon JE, Lindeman KG, Kim SC. Fracture risk after bariatric surgery: Roux-en-Y gastric bypass versus adjustable gastric banding. *J Bone Miner Res*. 2017;32(6):1229–1236.
11. Pizzorno L. Bariatric surgery: bad to the bone, part 2. *Integr Med (Encinitas)*. 2016;15(2):35–46.
12. Pizzorno L. Bariatric Surgery: Bad to the bone, part 1. *Integr Med (Encinitas)*. 2016;15(1):48–54.
13. Gregory NS. The effects of bariatric surgery on bone metabolism. *Endocrinol Metab Clin North Am*. 2017;46(1):105–116.
14. Abegg K, et al. Roux-en-Y gastric bypass surgery reduces bone mineral density and induces metabolic acidosis in rats. *Am J Physiol Regul Integr Comp Physiol*. 2013;305(9):R999–R1009.
15. Stemmer K, et al. Roux-en-Y gastric bypass surgery but not vertical sleeve gastrectomy decreases bone mass in male rats. *Endocrinology*. 2013;154(6):2015–2024.
16. Li Z, Hardij J, Bagchi DP, Scheller EL, MacDougald OA. Development, regulation, metabolism and function of bone marrow adipose tissues. *Bone*. 2018;110:134–140.
17. Scheller EL, Rosen CJ. What's the matter with MAT? Marrow adipose tissue, metabolism, and skeletal health. *Ann N Y Acad Sci*. 2014;1311:14–30.
18. Bailly L, Schiavo L, Sebastianelli L, Fabre R, Pradier C, Iannelli A. Anemia and bariatric surgery: results of a national French survey on administrative data of 306,298 consecutive patients between 2008 and 2016. *Obes Surg*. 2018;28(8):2313–2320.
19. McCabe LR, et al. Exercise prevents high fat diet-induced bone loss, marrow adiposity and dysbiosis in male mice. *Bone*. 2019;118:20–31.
20. Shu L, et al. High-fat diet causes bone loss in young mice by promoting osteoclastogenesis through alteration of the bone marrow environment. *Calcif Tissue Int*. 2015;96(4):313–323.
21. Schafer AL. Decline in bone mass during weight loss: a cause for concern? *J Bone Miner Res*. 2016;31(1):36–39.
22. Scheller EL, et al. Region-specific variation in the properties of skeletal adipocytes reveals regulated and constitutive marrow adipose tissues. *Nat Commun*. 2015;6:7808.
23. Yamada C, et al. The murine glucagon-like peptide-1 receptor is essential for control of bone resorption. *Endocrinology*. 2008;149(2):574–579.
24. Haderslev KV, et al. Short-term administration of glucagon-like peptide-2. Effects on bone mineral density and markers of bone turnover in short-bowel patients with no colon. *Scand J Gastroenterol*. 2002;37(4):392–398.
25. Ivaska KK, et al. Changes in bone metabolism after bariatric surgery by gastric bypass or sleeve gastrectomy. *Bone*. 2017;95:47–54.
26. Bredella MA, Greenblatt LB, Eajazi A, Torriani M, Yu EW. Effects of Roux-en-Y gastric bypass and sleeve gastrectomy on bone mineral density and marrow adipose tissue. *Bone*. 2017;95:85–90.
27. Fisher JE, et al. Alendronate mechanism of action: geranylgeraniol, an intermediate in the mevalonate pathway, prevents inhibition of osteoclast formation, bone resorption, and kinase activation in vitro. *Proc Natl Acad Sci USA*. 1999;96(1):133–138.
28. Zaidi M, et al. ACTH protects against glucocorticoid-induced osteonecrosis of bone. *Proc Natl Acad Sci USA*. 2010;107(19):8782–8787.
29. Ridelman E, Evers SS, Hoenerhoff MJ, Green JE, Seeley RJ. Alterations in serum-based breast cancer markers following bariatric surgery in rodent models: are they of clinical Value? *J Obesity and Bariatric Surgery*. Auctores Online Web site. https://www.auctoresonline.org/journals/obesity-and-bariatric-surgery/current-issue/375. Published August 23, 2018. Accessed March 28, 2019.
30. Winkler IG, et al. Bone marrow macrophages maintain hematopoietic stem cell (HSC) niches and their depletion mobilizes HSCs. *Blood*. 2010;116(23):4815–4828.
31. Carulli G. Effects of recombinant human granulocyte colony-stimulating factor administration on neutrophil phenotype and functions. *Haematologica*. 1997;82(5):606–616.
32. Pojda Z, Molineux G, Dexter TM. Hemopoietic effects of short-term in vivo treatment of mice with various doses of rhG-CSF. *Exp Hematol*. 1990;18(1):27–31.
33. Dunn SM, Coles LS, Lang RK, Gerondakis S, Vadas MA, Shannon MF. Requirement for nuclear factor (NF)-kappa B p65 and NF-interleukin-6 binding elements in the tumor necrosis factor response region of the granulocyte colony-stimulating factor promoter. *Blood*. 1994;83(9):2469–2479.
34. Cai XY, Gommoll CP, Justice L, Narula SK, Fine JS. Regulation of granulocyte colony-stimulating factor gene expression by interleukin-17. *Immunol Lett*. 1998;62(1):51–58.
35. Pojda Z, Molineux G, Dexter TM. Effects of long-term in vivo treatment of mice with purified murine recombinant GM-CSF. *Exp Hematol*. 1989;17(11):1100–1104.
36. Yu EW, Carmody JS, Brooks DJ, LaJoie S, Kaplan LM, Bouxsein ML. Cortical and trabecular deterioration in mouse models of Roux-en-Y gastric bypass. *Bone*. 2016;85:23–28.
37. Yu EW. Bone metabolism after bariatric surgery. *J Bone Miner Res*. 2014;29(7):1507–1518.
38. Pluskiewicz W, Bużga M, Holéczy P, Bortlík L, Šmajstrla V, Adamczyk P. Bone mineral changes in spine and proximal femur in individual obese women after laparoscopic sleeve gastrectomy: a short-term study. *Obes Surg*. 2012;22(7):1068–1076.
39. Muschitz C, et al. Sclerostin levels and changes in bone metabolism after bariatric surgery. *J Clin Endocrinol Metab*. 2015;100(3):891–901.
40. Yu EW, et al. Two-year changes in bone density after Roux-en-Y gastric bypass surgery. *J Clin Endocrinol Metab*. 2015;100(4):1452–1459.
41. Dixon JB, O'Brien PE. Obesity and the white blood cell count: changes with sustained weight loss. *Obes Surg*. 2006;16(3):251–257.
42. Dallal RM, Leighton J, Trang A. Analysis of leukopenia and anemia after gastric bypass surgery. *Surg Obes Relat Dis*. 2012;8(2):164–168.
43. Johansson HE, Haenni A, Zethelius B. Changes in erythrocyte sedimentation rate, white blood cell count, liver enzymes, and magnesium after gastric bypass surgery. *J Obes*. 2011;2011:273105.
44. Albanopoulos K, et al. C-reactive protein, white blood cells, and neutrophils as early predictors of postoperative complications in patients undergoing laparoscopic sleeve gastrectomy. *Surg Endosc*. 2013;27(3):864–871.
45. Kim TY, et al. Bone marrow fat changes after gastric bypass surgery are associated with loss of bone mass. *J Bone Miner Res*. 2017;32(11):2239–2247.
46. Schafer AL, et al. Changes in vertebral bone marrow fat and bone mass after gastric bypass surgery: A pilot study. *Bone*. 2015;74:140–145.
47. Takamatsu Y, Simmons PJ, Moore RJ, Morris HA,

To LB, Lévesque JP. Osteoclast-mediated bone resorption is stimulated during short-term administration of granulocyte colony-stimulating factor but is not responsible for hematopoietic progenitor cell mobilization. *Blood*. 1998;92(9):3465–3473.

48. Katayama Y, et al. Signals from the sympathetic nervous system regulate hematopoietic stem cell egress from bone marrow. *Cell*. 2006;124(2):407–421.

49. Scheller EL, et al. Bone marrow adipocytes resist lipolysis and remodeling in response to β-adrenergic stimulation. *Bone*. 2019;118:32–41.

50. Agarwal S, et al. G-CSF promotes neuroblasto-

ma tumorigenicity and metastasis via STAT3-dependent cancer stem cell activation. *Cancer Res*. 2015;75(12):2566–2579.

51. Chambers AP, et al. The role of pancreatic preproglucagon in glucose homeostasis in mice. *Cell Metab*. 2017;25(4):927–934.e3.

52. Patel A, Yusta B, Matthews D, Charron MJ, Seeley RJ, Drucker DJ. GLP-2 receptor signaling controls circulating bile acid levels but not glucose homeostasis in Gcgr. *Mol Metab*. 2018;16:45–54.

53. Merceron C, et al. Loss of HIF-1α in the notochord results in cell death and complete disappearance of the nucleus pulposus. *PLoS ONE*.

2014;9(10):e110768.

54. Morse A, et al. Mechanical load increases in bone formation via a sclerostin-independent pathway. *J Bone Miner Res*. 2014;29(11):2456–2467.

55. Sinder BP, Eddy MM, Ominsky MS, Caird MS, Marini JC, Kozloff KM. Sclerostin antibody improves skeletal parameters in a Brtl/+ mouse model of osteogenesis imperfecta. *J Bone Miner Res*. 2013;28(1):73–80.

56. Miller CA, et al. A case of acute myeloid leukemia with promyelocytic features characterized by expression of a novel . *Blood Adv*. 2018;2(11):1295–1299.